PAPER

Check for updates

Durable, rate-capable and high-energy hybrid supercapacitor from PANI/ZnO/SnO₂ nanocomposite with zero-waste electrolyte approach†

Aranganathan Viswanathan 🆔 * and Vanchiappan Aravindan*

A hybrid supercapacitor material, polyaniline/ZnO/SnO₂ of respective weight percentages of 58.34%:8.33%:33.33% (PZnSn), was synthesized by a facile *in situ* single-step method. Remarkably, the constituent ZnO was synthesized at 90 °C by this method along with the other two constituents in 2 h. This is astonishing because, the synthesis of ZnO generally involves calcination at high temperature for a longer duration. The energy storage performance was evaluated with two aqueous electrolytes: 1 M H_2SO_4 (SA) and the liquid by-product that was obtained after the synthesis of PANI (SLP). SLP provided 57.25% higher energy storage performance than that provided by SA. PZnSn showed its durability and rate-capable energy storage property by exhibiting robustness up to 16 500 cycles at 0.4 V s^{-1} and 39 A g^{-1} in the presence of (ITPO) SA and up to 15 000 cycles at 0.4 V s^{-1} and 42 A g^{-1}, respectively, ITPO SLP, in a real-time symmetric two-electrode system. PZnSn displayed the remarkable trait of enhancement of energy storage with an increase in the number of charge and discharge cycles ITPO both electrolytes. However, the enhancement provided by SLP is higher than that provided by SA. The maximum performance achieved from PZnSn ITPO SLP is a specific capacity (Q) of 347.2 C g^{-1}, a specific energy (E) of 57.87 W h kg^{-1} (comparable to Ni–Cd batteries) and a specific power (P) of 1.2 kW kg^{-1} at 1 A g^{-1}.

Introduction

Hybrid supercapacitors are devices that contain an electrode material that exhibits energy storage characteristics of both capacitive and battery types. Such materials are believed to impart high-energy characteristics closer to those of batteries in terms of their specific energy (E), with the high specific power (P) of capacitors and supercapacitors. This combination of the characteristics of both batteries and capacitors could be made by integrating both capacitive- or pseudocapacitive-type electrode materials with battery-type materials. A capacitive-type material involves surface capacitive processes (electrical double-layer formation and fast redox reactions) in energy storage, and a battery-type material involves bulk processes like intercalation. The combination of both surface and bulk energy storage processes is essential for achieving high-energy character in a charge storage device.

The best-known pseudocapacitive material and conducting polymer is polyaniline (PANI),[1,2] which is involved in the

Department of Chemistry, Indian Institute of Science Education and Research (IISER), Tirupati-517619, Andhra Pradesh, India. E-mail: ranguchemist@gmail.com, aravind.van@gmail.com

† Electronic supplementary information (ESI) available. See DOI: https://doi.org/10.1039/d4ya00617h

pseudocapacitive process through a redox transformation between its leucoemaraldine, emaraldine and pernigraniline forms.[3] In addition, it is inexpensive, facile to synthesize, environmentally friendly, non-toxic, and has a theoretical specific capacity (Q) of ~294 mA h g^{-1}.[4,5] SnO_2 is a known battery-type material[6–8] (with a theoretical Q of ~790 mA h g^{-1}),[9] easy to synthesize, and predominantly involves the bulk process of energy storage. ZnO is used in both batteries[10–13] and supercapacitors[14–19] due to its versatile nature, showing both pseudocapacitive-type and battery-type energy storage behavior. The synthesis of ZnO by a wet method at low temperature is not common, but it can be synthesized in a chemical reduction method, not as an individual entity but with other metal derivatives when the purpose of the synthesis is to produce a double metal oxide, as reported in our earlier study.[5] The electrolytes used in supercapacitors are as important as the other elements, because they play an essential role in determining the potential window and the quantity of energy stored in energy storage devices. The use of liquid by-products obtained after the synthesis of PANI as electrolyte was found to be an effective method of increasing the energy storage and the rate capability of supercapacitors.[20,21] The use of this liquid by-product from the synthesis of PANI exhibited 40%[21] and 22%[20] enhancements in energy storage in PANI-containing supercapacitors in relation to conventional 1 M H_2SO_4. Therefore, it is

intended to further explore the capability of this liquid by-product obtained from the synthesis of PANI in this study.

Herein, an attempt has been made to produce a hybrid supercapacitor electrode material by integrating PANI, ZnO and SnO$_2$ (PZnSn) by a facile *in situ* single-step method ITPO of two electrolytes, which are 1 M H$_2$SO$_4$ and the liquid by-product of the synthesis of PANI. As this combination can undergo EDL formation, pseudocapactive reactions with a higher number of electrons, and the bulk process of H$^+$ intercalation. It is anticipated that PZnSn will exhibit high-energy hybrid super-capacitor behavior. The synthetic method and structural and energy storage characterizations of PZnSn are provided in the following sections.

Experimental section

Synthesis of polyaniline, zinc oxide and stannic oxide (PANI/ZnO/SnO$_2$) (PZnSn) nanocomposite

The synthesis of the PZnSn composite was conducted based on the synthetic procedure given in in the granted Indian patent.[22] In the synthesis of PZnSn, 350 μL of aniline was mixed with 100 mL of distilled water (DW) and stirred for 15 min, then 1.4 g of ammonium persulfate dissolved in a minimum amount of DW was added, following which 10 mL of 2 M CH$_3$SO$_3$H was also added as a dopant and the reaction mixture was stirred at room temperature for 5 h. After 5 h of oxidative polymerization, the pH of the reaction mixture was raised to 14 using 6 M NaOH and then the reduction reaction of the mixture was carried out using an appropriate amount of hydrazine hydrate for 2 h at 90 °C. After 2 h of reduction, 13.27 mL of SnCl$_4$·5H$_2$O and 5 mL of ZnSO$_4$·7H$_2$O were mixed and stirred at 45 °C for 30 min. Then, the reaction mixture was cooled, and the targeted composite of PZnSn was extracted from the reaction mixture using the method mentioned in ref. 20. Thus, the PANI/ZnO/SnO$_2$ composite was obtained, and the weight composition of the composite was PANI 58.34%: ZnO 8.33%: SnO$_2$ 33.33%. The synthesis of PANI and its by-products are provided in the ESI† (Section S1) together with details of the characterization (S2) and fabrication (S3).

Uniqueness of the synthetic method

The synthesis of PANI/ZnO/SnO$_2$ is unique as it provides the composite containing ZnO at a lower temperature of 90 °C in 2 h without using any sophisticated setups or apparatus, because generally the synthesis of ZnO involves the synthesis of Zn(OH)$_2$ by treating a solution of zinc salt with a base like NaOH or KOH, and then calcinating Zn(OH)$_2$ at 500 °C to obtain ZnO.[23] ZnO is also synthesized using a hydrothermal method by heating Zn(OH)$_2$ at 150–200 °C in an autoclave.[24–26] The sol–gel method involves heating a sol–gel at 150 °C for 5 h;[27] the microemulsion method involves heating an emulsion at 140 °C for 5 h with a reflux condenser.[28] The solvothermal method involves heating at 120 °C for 5 h in a Teflon-lined stainless steel autoclave;[29] electrochemical deposition involves a three-electrode cell setup with the electrolyte consisting of a

mixture of Zn(NO$_3$)$_2$, KNO$_3$ and KCl at 80 °C;[30] one wet chemical method involves the heating of a mixture of aqueous solution Zn(NO$_3$)$_2$ and ammonia at 120 °C with a reflux condenser for 12 h;[31] the flux method involves the reagents for ZnO at temperatures in the range of 450 to 900 °C for 1 to 120 h;[32] the electrospinning method involves a mixture of PVA and zinc acetate, a high voltage of 20 kV, and high-temperature calcination at 500 °C for 4–10 h;[33] the microwave method involves exposure of the reagents for ZnO to microwaves produced at 510 to 680 W for 10 to 15 min;[34] and the polyol method involves heating the reagents for ZnO at 180 °C for 30 min.[35] Other than these solution-based methods, vapor-phase approaches are also available for synthesizing ZnO: molecular beam epitaxy (MBE), thermal evaporation, physical vapor deposition, plasma enhanced chemical vapor deposition (PECVD), chemical vapor deposition, metal–organic chemical vapor deposition (MOCVD), and pulsed laser deposition.[36] These methods also require sophisticated setup and apparatus. In addition, the synthesis of composites of ZnO with PANI generally involves two-step synthesis, that is, synthesizing PANI or a PANI-containing composite and then adding pre-synthesized ZnO or adding ZnO to PANI during its oxidative polymerization.[37–42] However, in this synthesis method, the composite of ZnO is made in a single step. Therefore, the presented method for the synthesis of ZnO composite is facile, unique, scalable and effective.

The use of the liquid by-product that is obtained after the synthesis of PANI as an electrolyte for supercapacitors is unique and beneficial, as proved in our early studies.[5,20,21] The use of the liquid by-product from PANI and a liquid by-product of synthesis of a composite electrode after acidification has enhanced energy storage and aided supercapacitors to move into the realm of batteries in terms of their specific energies. This waste-to-wealth approach not only enhances energy storage to a significant extent but also reduces the waste discharged into the environment and reduces the costs involved in the domains of energy storage and conversion.

Results and discussion

Structural characterization

The XRD pattern of PZnSn (Fig. 1a) contains peaks corresponding to the (002), (101), (200), (112) and (201) planes of ZnO (JCPDS No. 01-1136) at 34.35°, 36.20°, 66.38°, 67.92° and 68.95°, respectively (Fig. S1, ESI†). The peak corresponding to the (211) plane of of SnO$_2$ is seen at 51.74 (JCPDS No. 41-1445).

The peak at 26.95° arises from both the (110) plane of SnO$_2$ and the (003) plane of PANI (JCPDS No. 53-1717) (Fig. S2, ESI†). The peak at 31.69° corresponds to both the (100) plane of ZnO and the (020) plane of PANI. The peak at 47.50° corresponds to both the (102) plane of ZnO and the (313) plane of PANI (Fig. S3, ESI†). Thus, the characteristic peaks of the constituents confirm the successful synthesis of the PZnSn composite. The FT-IR peak positions and their corresponding species are presented in ESI† (Section S3). The Raman peaks (Fig. 1c) at
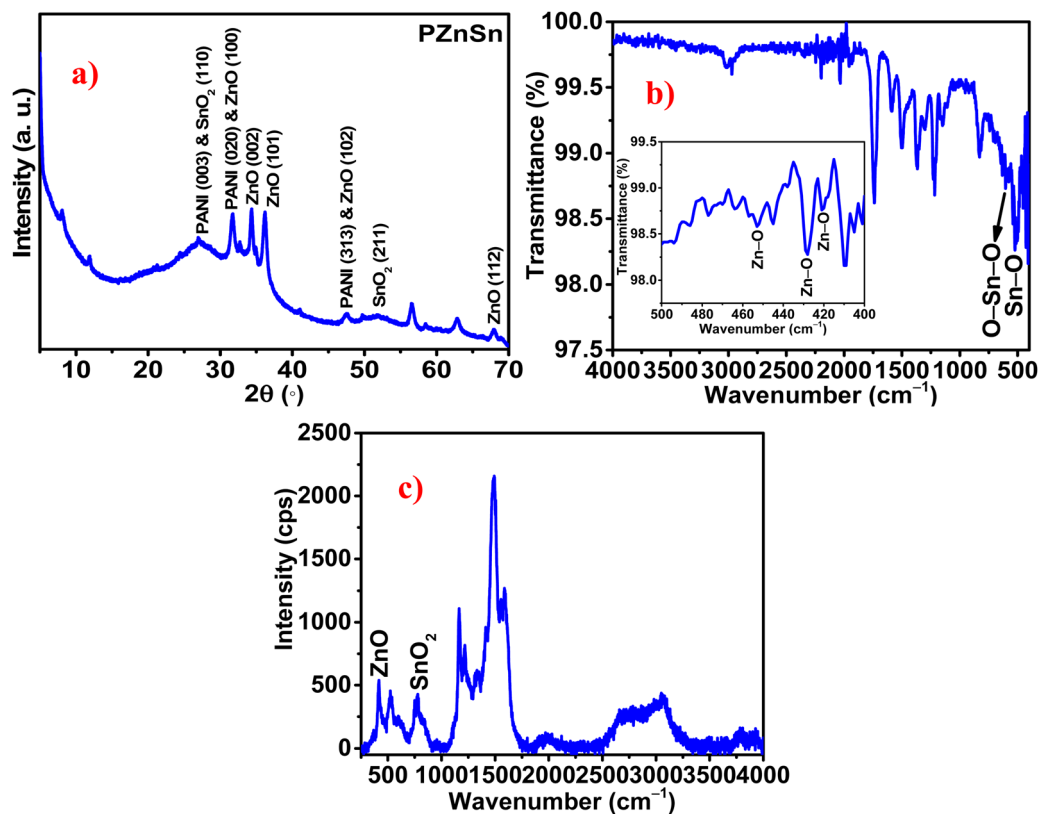
Fig. 1 (a) XRD pattern, (b) FT-IR, and (c) Raman spectrum of PZnSn.

415 cm^{-1} (E$_1$)[43] and 778 cm^{-1} (B$_{2g}$)[44] correspond to ZnO and SnO$_2$, respectively. The peaks at 1163, 1217, and 1491 cm^{-1} are due to the C–H of the benzenoid rings, the C–N stretching of the poloranic segments[44] and the C=N stretching vibrations of the

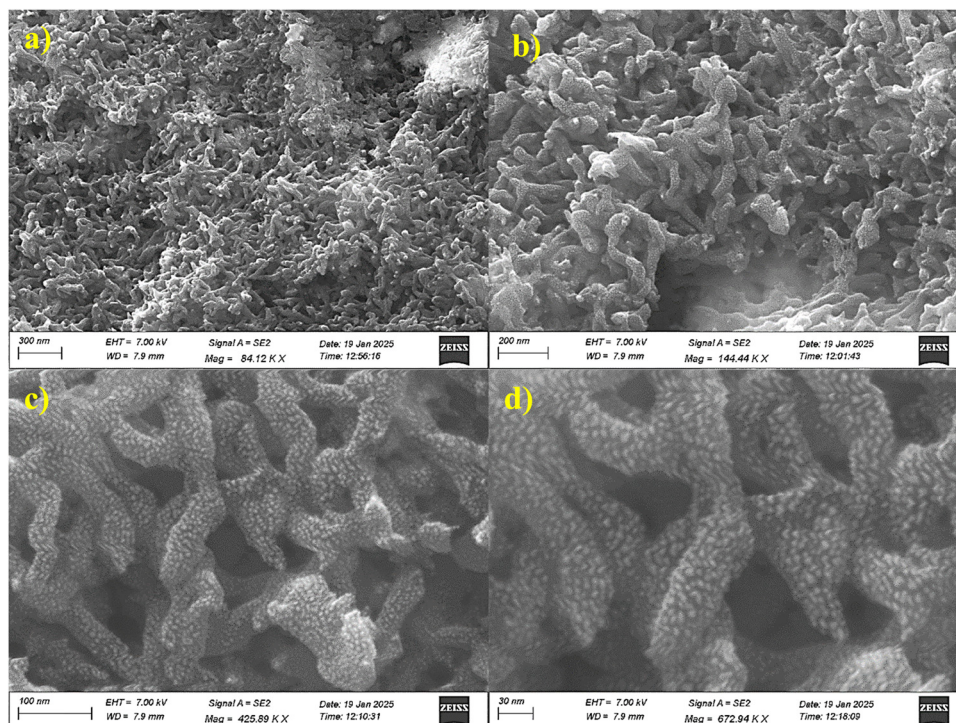

Fig. 2 (a)–(d) FE-SEM images of PZnSn at different magnifications.

quinoid rings[45] of PANI, respectively. The peaks at 1332, 1412, 1556 and 1586 cm^{-1} are also due to different vibrations of PANI.[44]

The FE-SEM images (Fig. 2) depict the morphology of PZnSn, in which PANI is seen to be morphologically fibrous and the nanoparticles of ZnO and SnO$_2$ are well dispersed upon the PANI fibers. PZnSn also has pores across its morphology to facilitate effective electrolytic permeation across the PZnSn nanocomposite. The diameter range of the PANI nanofibers coated with ZnO and SnO$_2$ is 38 to 54 nm, and that of the pores is 59 to 88 nm (Fig. S4, ESI†). The elemental maps (Fig. S5, ESI†) of PZnSn evidently depict the effective dispersion of the elements and, in turn, the constituents across the PZnSn composite.

The XPS survey spectrum of the PZnSn (Fig. 3a) composite contains the characteristic peaks of the elements of PZnSn. The chemical nature of the elements was deduced from the deconvolution process of the core-level spectrum of each element. The peaks obtained in the deconvolution process and the respective chemical nature of their elements confirm that the chemical forms of the elements present in PZnSn are PANI, ZnO and SnO$_2$ (Table 1).

Electrochemical characterization

The energy storage performance of the PZnSn composite was assessed in a 2-electrode (2-EL) system using 1 M H$_2$SO$_4$ (SA) and the liquid by-product obtained after the synthesis of PANI (SLP) as electrolytes. The energy storage study of the PZnSn composite revealed that PZnSn exhibits promising energy storage characteristics and exhibits the remarkable trait of increase in energy storage with an increase in the number of cycles ("increase in number of cycles" is abbreviated to INC) during the cyclic
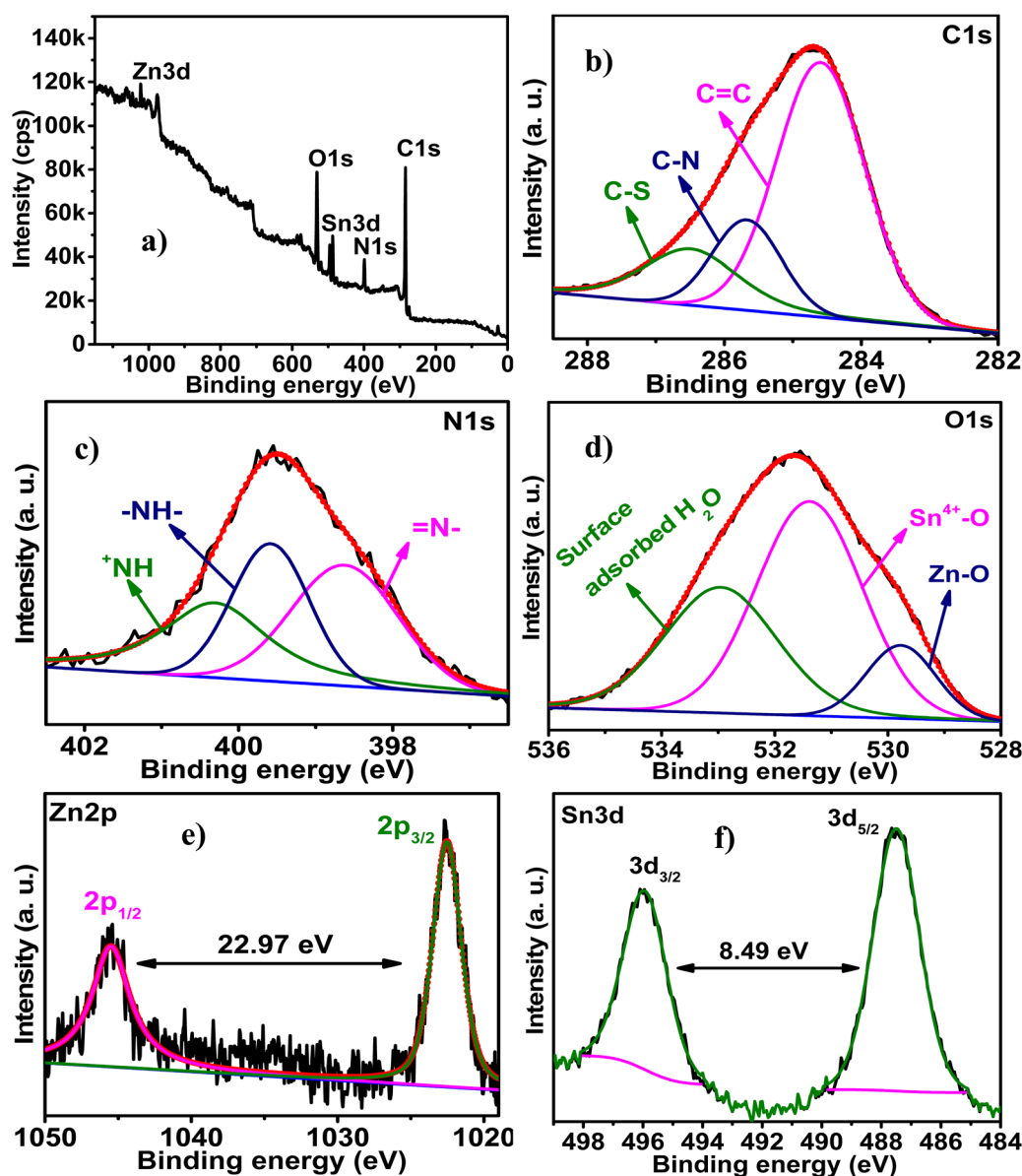

Fig. 3 XPS (a) survey spectrum and core-level spectra of (b) C 1s, (c) N 1s, (d) O 1s, (e) Zn 2p and (f) Sn 3d of PZnSn.

Table 1 XPS peak positions and their respective chemical species

Element	Binding energy (eV) and species
C 1s	284.60 eV (C=C), 285.7 eV (C–N) and 286.53 eV (C–S)[44] (Fig. 3a)
N 1s	398.63 eV (=N–), 399.58 eV (–NH–) and 400.32 eV ($^+$NH)[3] (Fig. 3b)
O 1s	529.79 eV (Zn–O),[46,47] 531.39 eV (Sn^{4+}–O)[44] and 532.98 eV (surface absorbed H_2O)[44] (Fig. 3c)
Zn 2p	1022.53 eV ($2p_{3/2}$)[48] and 1045.5 eV ($2p_{1/2}$) (doublet energy difference: 22.97 eV)[49] (Fig. 3d)
Sn 3d	487.49 eV ($3d_{5/2}$)[50] and 495.98 eV ($3d_{3/2}$)[51] (doublet energy difference: 8.49 eV)[52] (Fig. 3e)

stability study at 0.4 V s^{-1} ITPO both electrolytes. This unique trait is not new, as similar observations have been made in the past with our other materials.[3,5,20,53–56] The energy storage enhancement obtained ITPO SLP is higher than that ITPO SA. In addition, the maximum performance of PZnSn ITPO SLP was obtained relatively quickly compared to that ITPO SA. The durability studies were conducted at 0.4 V s^{-1}, up to 16 500 and 15 000 cycles ITPO SA and SLP, respectively. The maximum performance of PZnSn occurred after 16 500 and 10 000 cycles ITPO SA and SLP, respectively. The higher energy storage obtained ITPO SLP suggests the efficient reuse of the liquid by-product of PANI as an electrolyte, reinforcing the point of "waste-to-wealth".

The unique characteristics of the increase in energy storage (eqn (S1), ESI†) with INC were characterized at different points of the cyclic stability test: before the cyclic study, after 4000, 10 000, and 16 500 cycles for SA and before cyclic study, after 5000, 10 000 and 15 000 cycles for SLP. In the following paragraphs, these "different number of cycles" are abbreviated to DNC and. The energy storage parameters like Q (eqn (S2)), E (eqn (S3)), specific power (P) (eqn (S4)), and Coulombic efficiency (η) (eqn (S5), ESI†) of PZnSn obtained after DNC ITPO SA and SLP are shown in Tables 2 and 3, respectively.

As shown in Table 2, with INC, Q is increasing, but η is decreasing ITPO SA. At the end of 16 500 cycles, the obtained η is 47.81%, which is lower for supercapacitors and, therefore, the cyclic stability test for SA was paused at this point. In the case of SLP, the energy storage performance begins to deteriorate after 10 000 cycles; therefore, it was stopped after 15 000 cycles. The entire findings and corresponding discussion of PZnSn are given in the following.

The higher faradaic area and longer discharge time (t_d) of PZnSn obtained ITPO SLP can be seen in Fig. 4a and b,

respectively. These higher faradaic areas and t_d indicate the higher energy storage ITPO SLP. The peaks and plateaus of the CV plots and charge–discharge (CD) plots of PZnSn indicate its faradaic process of energy storage. As it can be seen in Fig. 4a, PZnSn exhibited a new faradaic peak ITPO SLP, which is attributed to the production of another intercalation process (Fig. 4f) in the potential range 0.35–0.55 V, which is an advantage of using SLP and which in turn increased the energy brought by it. The Q of PZnSn at 1 A g^{-1} ITPO SA and SLP are 162 and 255 C g^{-1}, respectively. The Q of PZnSn obtained ITPO SLP is 57.25% higher than that obtained ITPO SA. This is due to the higher occurrence of diffusion-controlled intercalation reactions ITPO SLP than that ITPO SA. The percentage contributions of surface capacitive processes (EDL + redox reaction) and diffusion-controlled intercalation processes to the energy storage of PZnSn ITPO SA (Fig. 4c and d) and SLP (Fig. 4e and f) were obtained by the deconvolution of the CV curves (eqn (S6) and (S7), ESI†). The percentage of energy stored by capacitive processes and intercalation reactions ITPO SA are 36.36 and 63.64%, respectively, and that ITPO SLP are 20.79 and 79.21%, respectively. This higher percentage of intercalation reactions occurring in ITPO SLP causes a higher Q in PZnSn in its presence.

The sustainability of PZnSn under higher potential and current loadings is studied by subjecting it to different potential scans and current densities. PZnSn ITPO both SA and SLP sustains a high potential scan of 0.2 V s^{-1} (Fig. S6a, ESI† and Fig. 5a). In the case of the CD study, PZnSn is sustained up to current densities of 14 and 32 A g^{-1} ITPO SA and SLP, respectively (Fig. S6b, ESI,† Fig. 5b and c).

The high current sustainability of PZnSn ITPO SLP indicates the better reversibility of energy storage reactions and the lowest amount of structural degradation that are taking place at higher current loadings in its presence. The Q obtained at 1 and 14 A g^{-1} ITP of SA are 162 and 28 C g^{-1} (17.28% retention), respectively (Fig. 5c).

The Q obtained at 1, 14 and 32 A g^{-1} ITPO SLP are 255, 112 (43.93% retention) and 31 C g^{-1} (12.05% retention), respectively. The high rate capability of PZnSn ITPO SLP indicates better electrolytic diffusion and a similar amount of energy storage reactions even at higher current loadings to those at lower current loadings. The plots of P vs. E (Fig. 5d) of PZnSn also follow a similar trend to that in Fig. 5c. The values of E and P obtained at 1 A g^{-1} are 27.01 W h kg^{-1} and 1.2 kW kg^{-1} ITPO SA and 42.49 W h kg^{-1} and 1.2 W h kg^{-1} ITPO SLP, respectively. The higher E obtained ITPO SLP is of the same order as those of Pb-lead acid and Ni–Cd batteries[57] (Fig. 5d).

Table 2 The energy storage parameters of PZnSn ITPO SA after DNC at 1 A g^{-1}

PZnSn	Q (C g^{-1})	E (W h kg^{-1})	P (kW kg^{-1})	η (%)
Before cyclic study	162.1	27.01	1.2	91.63
After 4000 cycles	169.7	28.28	1.2	84.02
After 10 000 cycles	243.8	40.64	1.2	70.24
After 16 500 cycles	312.0	52.00	1.2	47.81

Table 3 The energy storage parameters of PZnSn ITPO SLP after DNC at 1 A g^{-1}

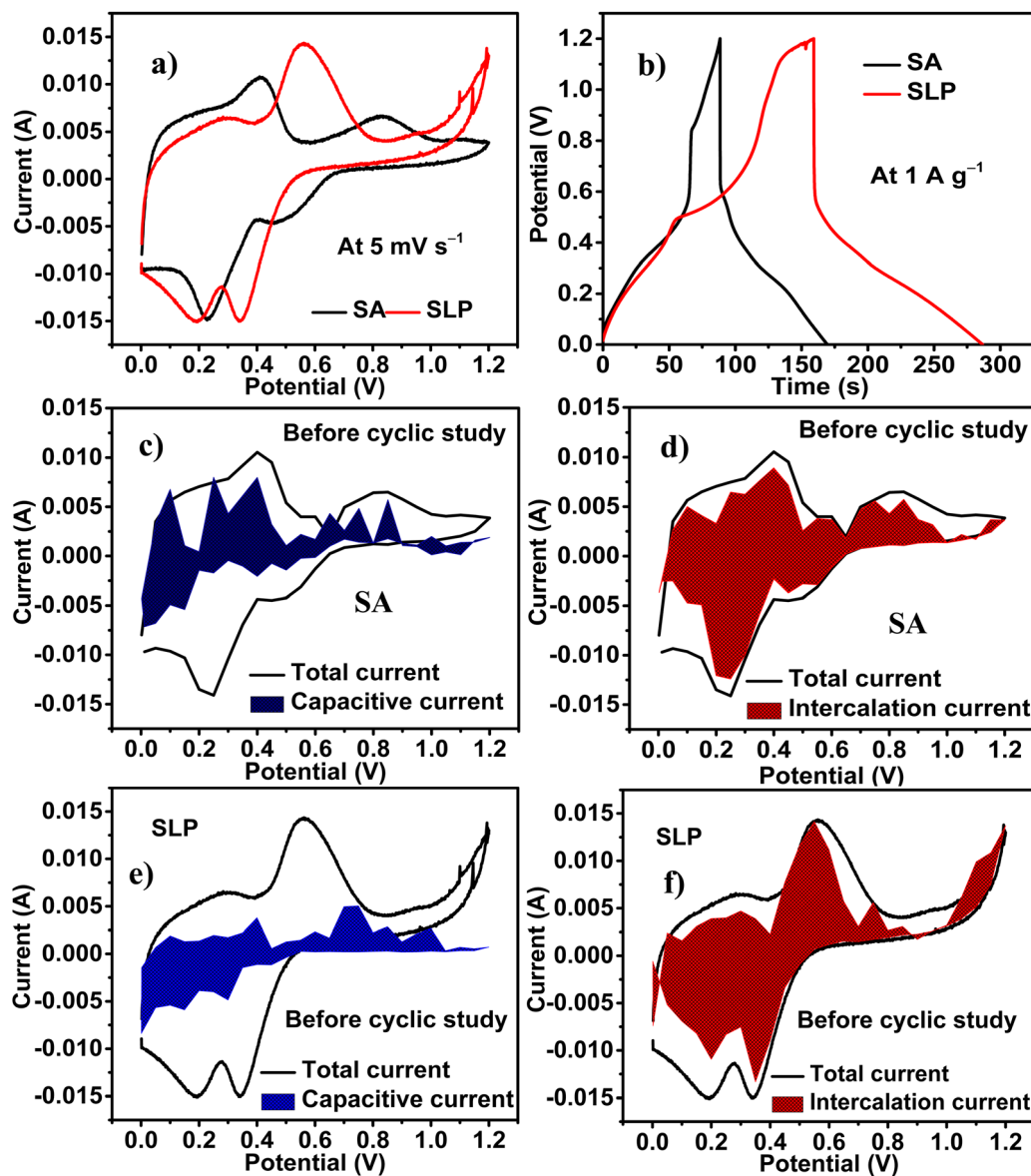| PZnSn	Q (C g^{-1})	E (W h kg^{-1})	P (kW kg^{-1})	η (%)
Before cyclic study	254.9	42.49	1.2	80.08
After 5000 cycles	308.6	51.43	1.2	77.69
After 10 000 cycles	347.2	57.87	1.2	59.85
After 15 000 cycles	288.3	48.06	1.2	68.69

Fig. 4 (a) CV plots at 5 mV s^{-1}, (b) charge and discharge (CD) plots at 1 A g^{-1} of PZnSn ITPO SA and SLP, (c) and (d) capacitive and intercalation current offered by PZnSn ITPO SA at 5 mV s^{-1}, (e) and (f) capacitive and intercalation current offered by PZnSn ITPO SLP at 5 mV s^{-1}.

The presence of SA provides higher η at all current densities in PZnSn than that obtained ITPO SLP. The low η of PZnSn ITPO SLP is due to the higher occurrence of intercalation reactions with lower kinetics than that ITPO SA. In both electrolytic cases, η increases with an increase in current density and reaches 100% at higher current densities (Fig. 5e). The cyclic stability of PZnSn was evaluated ITPO both electrolytes at 0.4 V s^{-1} (Fig. 5f).

The change in Q (eqn (S1), ESI†) as a function of INC exhibits a trend of peaks and valleys in the cases of both electrolytes, but the extent of the peaks and valleys is lower in the case of SLP, which indicates that SLP shows greater compatibility with PZnSn. This stability ITPO SLP also signifies the robustness and reversibility of the energy storage reactions of PZnSn ITPO SLP. However, an overall increase in Q is

observed (Fig. 5f). During the cyclic stability test, the consecutive increase and decrease in Q are attributed to the simultaneous structural breakdown and self-healing of the emaraldine salt form of PANI.[58] The reason for the increase in Q with INC is that the continuous insertion and extraction of ions of SA and SLP increase the intercalation processes of PZnSn. This increase in intercalation processes is the main reason for the increase in Q with INC. This intercalation process occurs until the electrode material is structurally damaged. This continuous diffusion of electrolytes unites the discrete parts of PZnSn, and thus, the surface of the electrode material taking part in energy storage increases. Once material damage occurs, the extent of energy storage reactions decreases, leading to a reduction in the amount of energy stored. Once the self-healing property of emaraldine form of PANI ceases, a continuous decrease in Q is
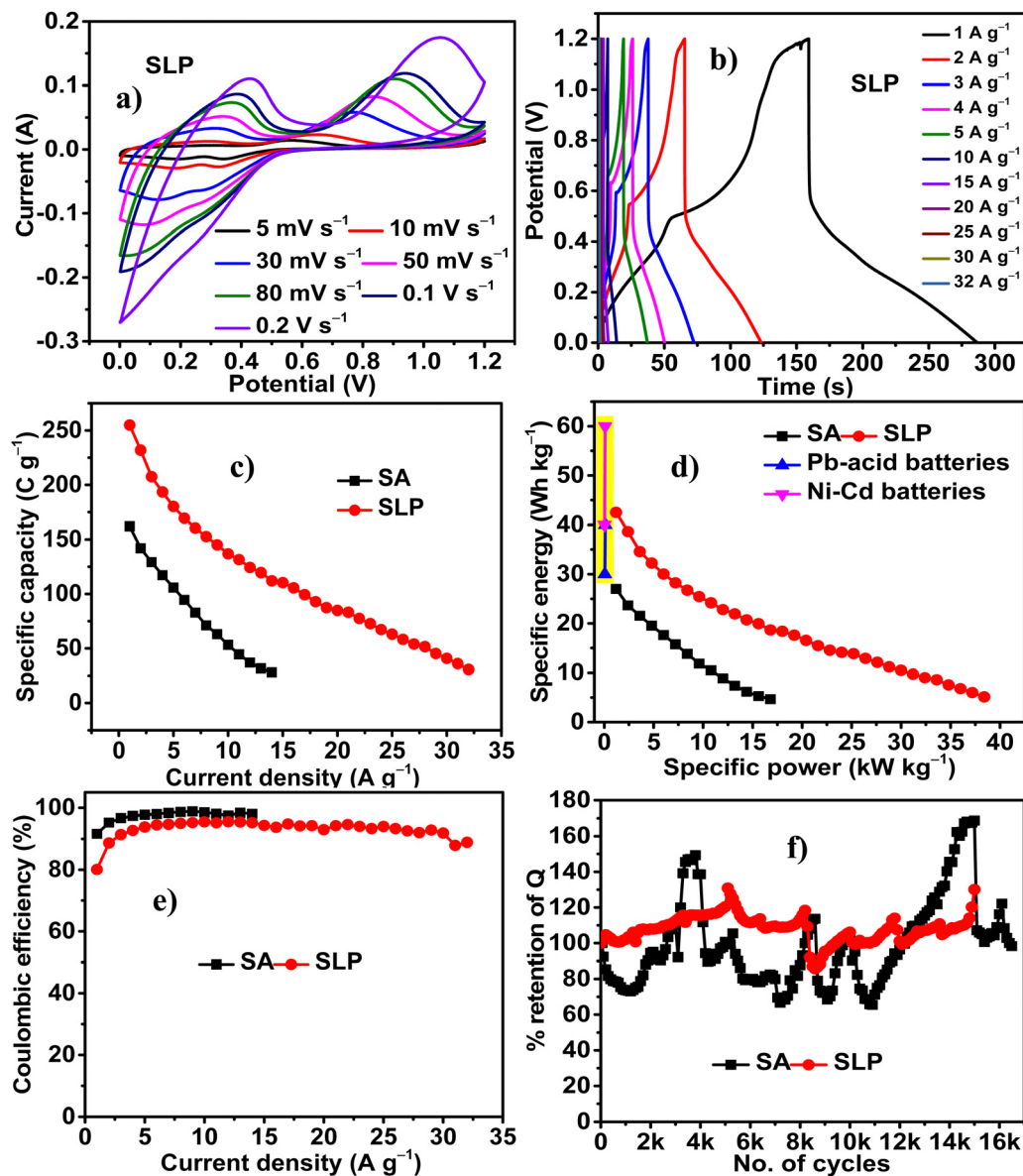
Fig. 5 (a) CV curves at different scan rates and (b) CD curves at different current densities of PZnSn ITPO SLP. (c) Plots of specific capacity *vs.* current density, (d) plots of specific energy *vs.* specific power, (e) plots of Coulombic efficiency *vs.* current density, and (f) % retention of *Q* *vs.* number of cycles.

observed due to the complete conversion of all emeraldine (half-reduced and half-oxidized form) to pernigraniline (completely oxidized form).[20] The plots of *b*-value *vs.* potential of PZnSn obtained ITPO SA (Fig. 6a) and SLP (Fig. 6b), after DNC, substantiate this rationalisation.

A comparison of the plots of *b*-value *vs.* potential (Fig. 6a and b) and CV curves obtained after DNC ITPO SA (Fig. S7) and SLP (Fig. S8, ESI†) evidently show that the intense peaks present in the CV profiles of PZnSn ITPO both electrolytes are due to the intercalation processes, as they possess *b*-values (eqn (S8), ESI†) closer to 0.5. In addition, with INC, the current produced by these intercalation peaks increases, indicating the enhanced occurrence of intercalation processes. As intercalation is a bulk process, it stores higher energy than redox reactions and the EDL formation process, which are surface phenomena. With

INC, the quasi-reversibility of the faradaic reactions increases, and this quasi-reversibility is attributed to the structural breakdown of PZnSn, which causes internal resistance. Due to this quasi-reversibility and internal resistance, *η* decreases with INC in the cases of both electrolytes. This above-mentioned internal resistance is seen in the form of an increased drop in IR with INC, which will be discussed in successive sections.

The deconvolutions of the CV curves that are obtained after 16 500 cycles and 10 000 cycles ITPO SA (Fig. 6c and d) and SLP (Fig. 5f and 6e), respectively, provide the percentage of energy stored by capacitive processes (eqn (S7), ESI†) (EDL + redox reaction) and intercalation reactions as 27.17 and 72.83%, and 21 and 79%, respectively. In the case of SA, the percentages of intercalation reactions increase with INC, as indicated by the quantity of intercalation contribution after 16 500 cycles,
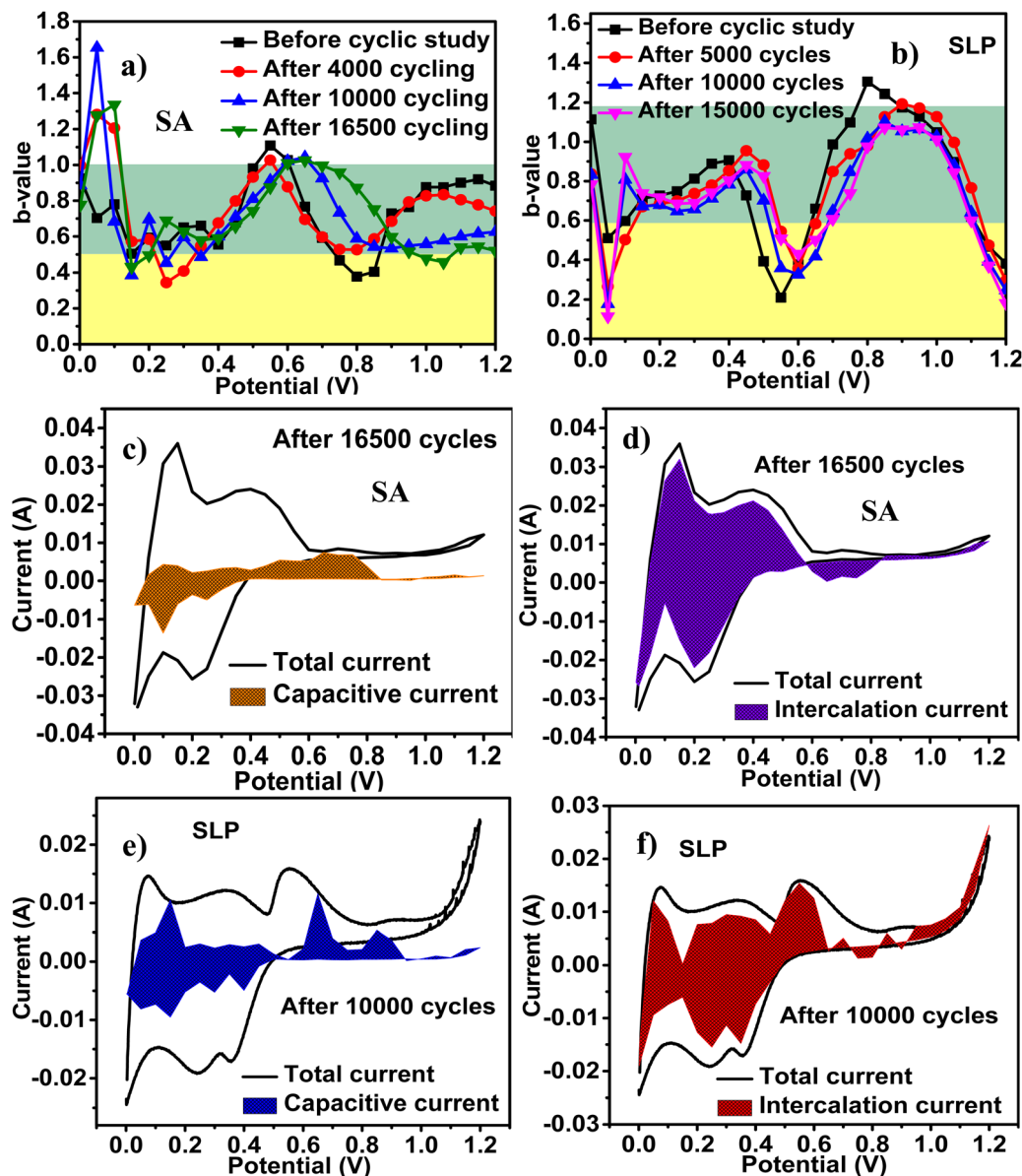
Fig. 6 Plots of b-value vs. potential of PZnSn ITPO (a) SA & (b) SLP after DNC. The deconvolution of the CV curve of PZnSn ITPO SA was obtained after 16 500 cycles, providing (c) capacitive current and (d) intercalation current. The deconvolution of the CV curve of PZnSn ITPO SLP was obtained after 10 000 cycles, providing (e) capacitive current and (f) intercalation current.

whereas, in the case of SLP, the percentages of capacitive and intercalation contributions remain intact in terms of quantity; however, their magnitudes have increased, as indicated by the migration of the b-values closer to the value of 0.5 (Fig. 6b) and the increase in the intensities of the CV peaks with INC. Through this combined occurrence of all three energy storage processes – EDL formation, redox reaction and intercalation reactions – to a relatively higher extent, ITPO SLP brings about higher energy storage in PZnSn, in relation to that ITPO SA. As can be seen in Fig. 6a and b, with INC, the potential range involved in the intercalation reaction increases; thus, the potential regions that are involved in the intercalation reaction are 0–0.4 V (Fig. 6a) and 0–0.8 V (Fig. 6b) in the cases of SA and SLP, respectively. This long-order intercalation reaction ITPO

SLP brings about higher energy storage in PZnSn in its presence.

The increase in the area of the faradaic peaks and discharge time (t_d) of the CV curves (Fig. 7a and b) and discharge curves (Fig. 7c and d), respectively, of PZnSn ITPO SA and SLP obtained after DNC indicate the increase in energy storage with INC. The high CV area and t_d (Fig. S9a and b, ESI†) of PZnSn obtained after 16 500 and 10 000 cycles indicate the maximum energy stored in it after 16 500 and 10 000 cycles ITPO SA and SLP, respectively.

The sustainability of the PZnSn under the high applied potential and current, even after 16 500 cycles (Fig. 8a and b) and 10 000 cycles (Fig. 8c and d) ITPO SA and SLP, respectively, is evident. The PZnSn consistently exhibits faradaic nature even
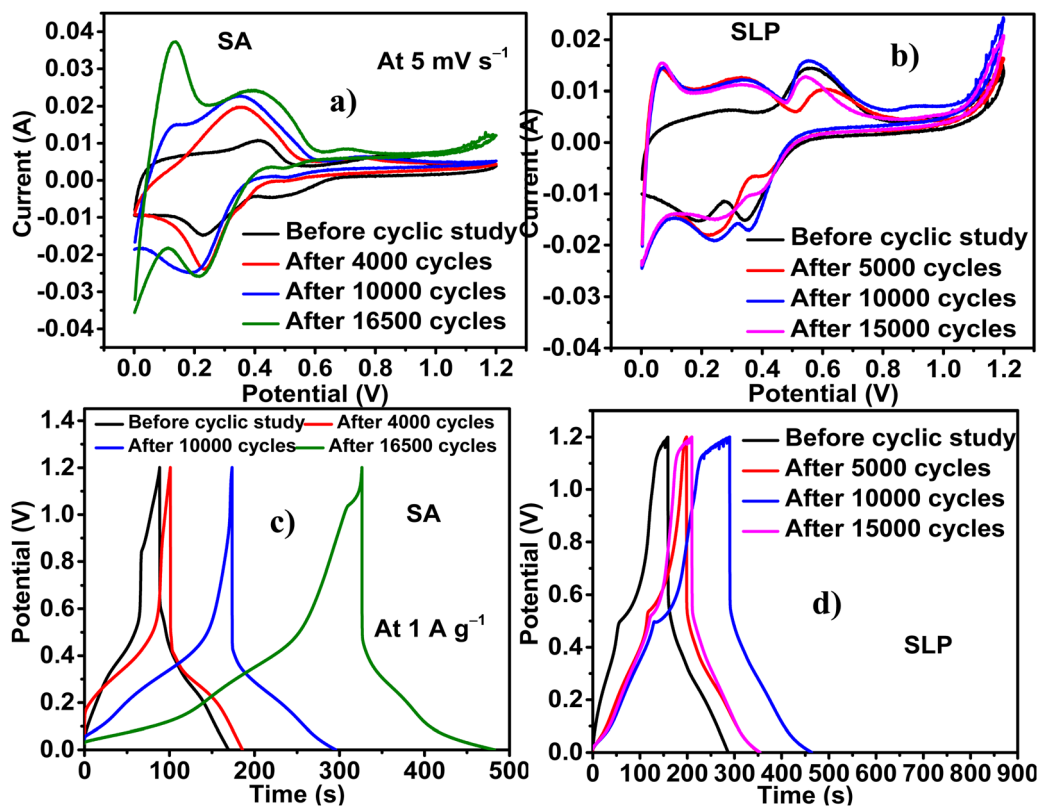
Fig. 7 CV plots of PZnSn after DNC at 5 mV s^{-1} ITPO (a) SA & (b) SLP. CD plots of PZnSn after DNC at 1 A g^{-1} ITPO (c) SA & (d) SLP.
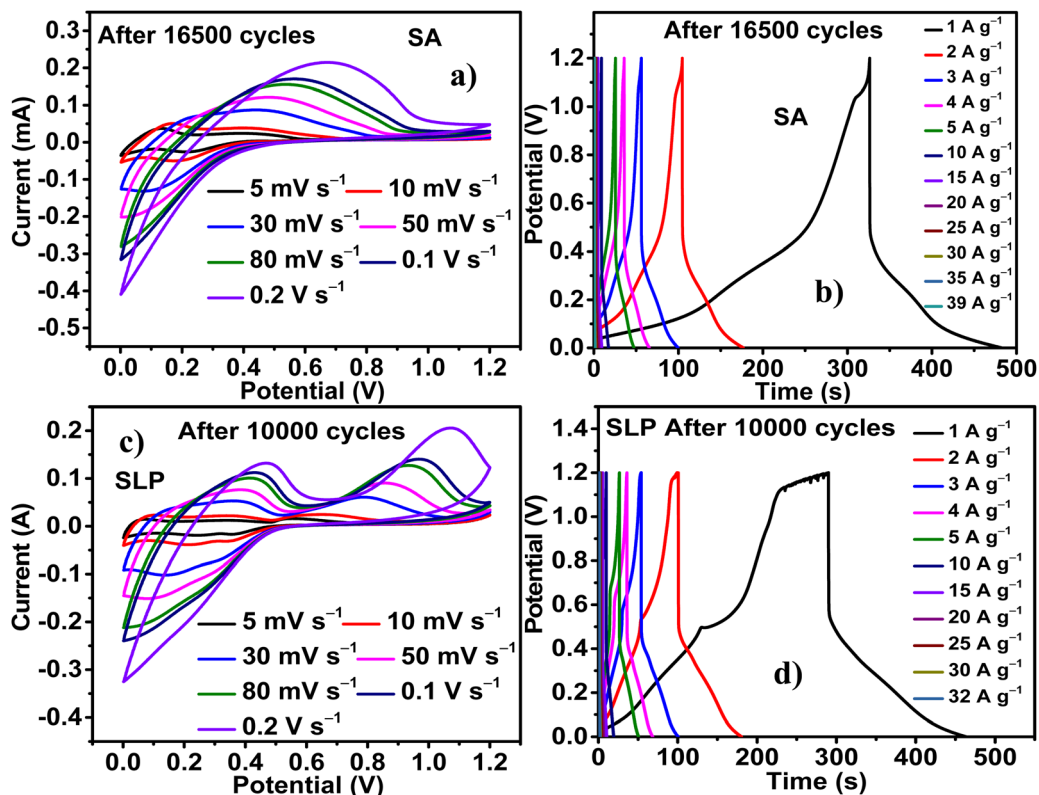

Fig. 8 (a) CV plots at different scan rates and (b) CD plots at different current densities of PZnSn after 16 500 cycles ITPO SA, (c) CV plots at different scan rates, and (d) CD plots at different current densities of PZnSn after 10 000 cycles ITPO SLP.

up to 0.2 V s^{-1} and 39 A g^{-1} in the case of SA and up to 0.2 V s^{-1} and 32 A g^{-1} in the case of SLP. It should be remarked that after 5000 cycles, PZnSn is consistent in exhibiting a faradaic nature up to 42 A g^{-1}, which is the highest current tolerance obtained ITPO SLP. This decrease in current tolerance exhibited by PZnSn ITPO SLP after 10 000 cycles indicates an increase in the quasi-reversibility of energy storage reactions and an increase in diffusional resistance due to the slight structural deformation in PZnSn with INC. The drops in IR observed after 0, 4000, 10 000, and 16 500 cycles ITPO SA are 0.2735, 0.3477, 0.3456 and 0.2741 V, respectively. Similarly, the IR drop observed before cyclic study and after 5000, 10 000, and 15 000 cycles ITPO SLP are 0.17, 0.22, 0.21 and 0.22 V, respectively. This trend of increase in IR drop in both cases is not so significant; therefore, a tradeoff between the slight structural deformation and the continuous enhancement in diffusion of electrolytes, causing an increase in intercalation reactions and bringing about higher energy storage with INC, is implied. The relatively low drop in IR exhibited by PZnSn ITPO SLP indicates the enhanced conductivity and better diffusion of ions of SLP into PZnSn in comparison with SA.

Fig. 9a depicts the increase in Q, sustainability to applied current and rate capability of PZnSn with INC ITPO SA. The values of Q obtained ITPO SA at 1 A g^{-1} before the cyclic study and after 4000, 10 000 and 16 500 cycles are 162, 169, 243, and 312 C g^{-1}, respectively. The maximum current tolerance exhibited by PZnSn ITPO SA before the cyclic stability study and after 4000, 10 000 and 16 500 cycles are 14, 25, 28 and 39 A g^{-1}, respectively. The retentions of the initial Q exhibited by PZnSn ITPO SA at 14 A g^{-1} are 17.28, 44.88, 43.86 and 45.23%, before the cyclic stability study and after 4000, 10 000 and 16 500 cycles, respectively. The retentions of the initial Q exhibited by PZnSn ITPO SA at the maximum current densities of 25, 28, and 39 A g^{-1} are 28.88, 23.43 and 12% after 4000, 10 000 and 16 500 cycles, respectively. The increase in Q and the rate capability are attributed to the higher magnitude of porosities present on the surface of PZnSn, causing better electrolyte permeation into PZnSn with INC and enabling promising diffusion of the electrolyte into PZnSn even at higher current densities, as occurs at lower current densities. The plots of E vs. P (Fig. 8b) show a similar trend to that of Fig. 8a. The maximum E obtained from PZnSn ITPO SA at 1 A g^{-1} and at a P of 1.2 kW kg^{-1} are 27.01, 28.28, 40.64 and 52 W h kg^{-1} before the cyclic study and after 4000, 10 000 and 16 500 cycles, respectively.

The values of η (Fig. 8c) obtained from PZnSn ITPO SA at 1 A g^{-1} are 93.63, 84.02, 70.24 and 47.81%, before the cyclic study and after 4000, 10 000 and 16 500 cycles, respectively. As the current density increases, η also increases and reaches the maximum of 100% at higher current densities during all points of cycling. The decrease in η with INC is ascribed to the increase
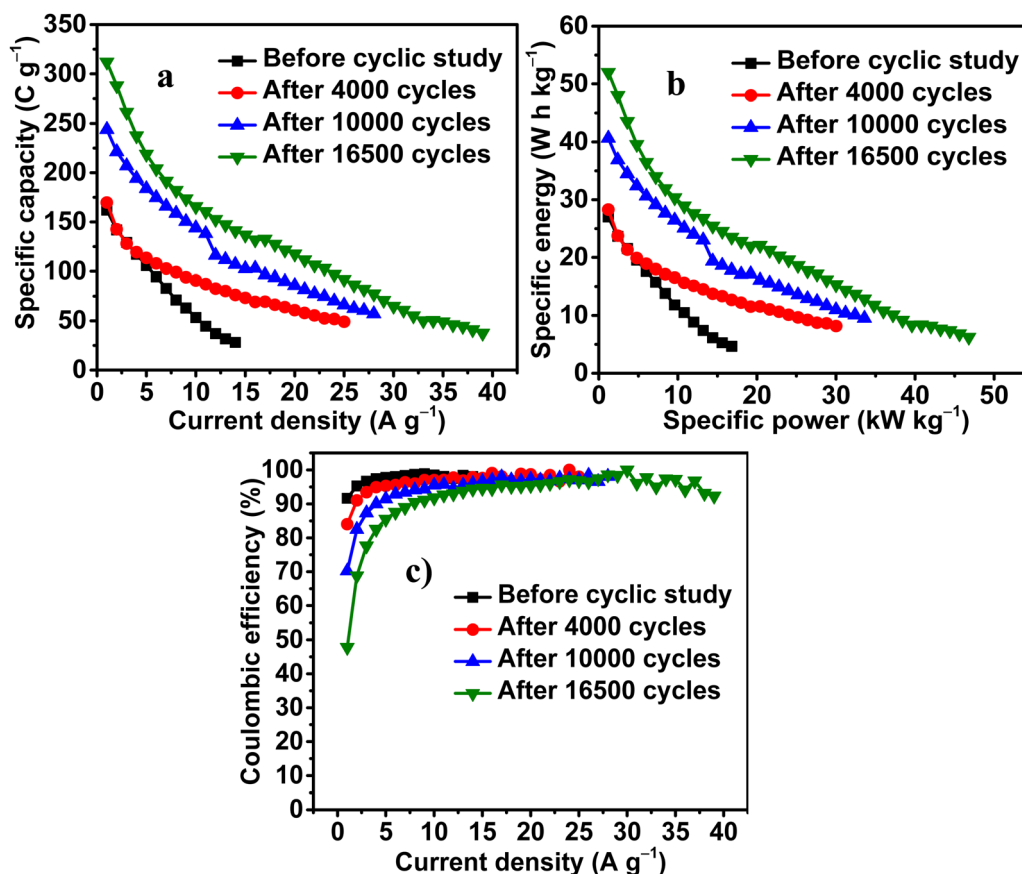

Fig. 9 Plots of (a) specific capacity vs. current density, (b) specific energy vs. specific power, and (c) Coulombic efficiency vs. current density of PZnSn obtained after DNC ITPO SA.

Fig. 10 Plots of (a) specific capacity *vs.* current density, (b) specific energy *vs.* specific power, and (c) Coulombic efficiency *vs.* current density of PZnSn obtained after DNC ITPO SLP.
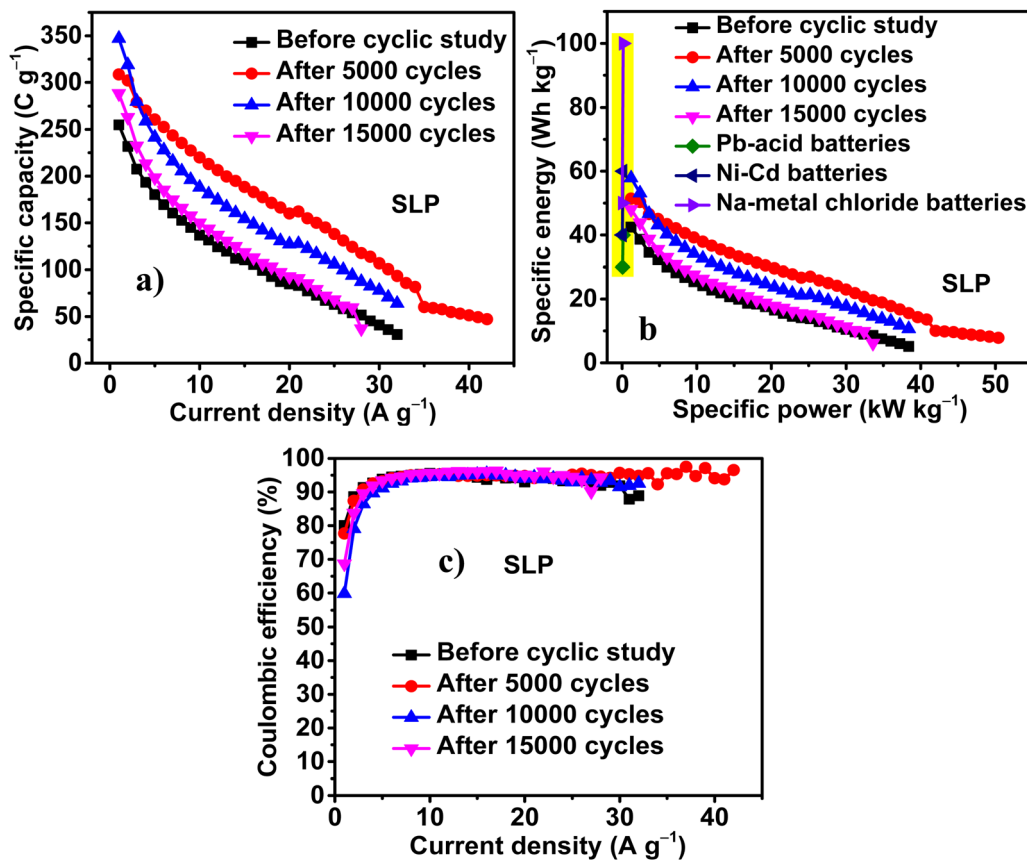
in the extent of intercalation processes, whose kinetics are lower than those of surface capacitive processes and the increase in quasi-reversibility of the energy storage processes. After 16 500 cycles, the obtained η is a minimum, which indicates the occurrence of a greater extent of intercalation, the higher energy storage caused by it and higher quasi-reversibility. This quasi-reversibility can be seen in the form of *b*-values with a magnitude of more than one at lower potentials (Fig. 6a), and that region corresponds to the inter-calation processes (Fig. 6d).

Fig. 10a depicts the increase in Q, sustainability to applied current and rate capability of PZnSn with INC ITPO SLP. The values of Q obtained ITPO SLP at 1 A g^{-1} before the cyclic study and after 5000, 10 000 and 15 000 cycles are 255, 309, 347, and 288 C g^{-1}, respectively. The maximum current tolerance exhibited by PZnSn ITPO SLP before the cyclic stability study and after 5000, 10 000 and 15 000 cycles are 32, 42, 32 and 28 A g^{-1}, respectively. The retentions of initial Q exhibited by PZnSn ITPO SLP at 28 A g^{-1} are 20.21, 38.11, 25.16 and 12.82% before the cyclic stability study and after 5000, 10 000 and 15 000 cycles, respectively. The retentions of initial Q exhibited by PZnSn ITPO SLP at the maximum current densities of 32, 42, and 32 A g^{-1} are 12.05, 15.24 and 18.43%, before the cyclic study and after 5000 and 10 000 cycles, respectively. The increase in Q and the rate capability ITPO SLP in relation to

SA is attributed to the greater permeation of electrolyte into PZnSn with INC, enabling the promising diffusion of electrolyte into the pores of PZnSn even at higher current densities, as occurs at lower current densities in comparison with SA. The plots of E *vs.* P (Fig. 10b) show a similar trend to that of Fig. 10a. The maximum E obtained from PZnSn ITPO SLP at 1 A g^{-1} and at a P of 1.2 kW kg^{-1} are 42.49, 51.43, 57.86 (comparable with Ni–Cd batteries) and 48.06 W h kg^{-1} before the cyclic study and after 5000, 10 000 and 15 000 cycles, respectively. The values of η (Fig. 10c) obtained from PZnSn ITPO SLP at 1 A g^{-1} are 80.07, 77.69, 59.84 and 68.68%, before the cyclic study and after 5000, 10 000 and 15 000 cycles, respectively. The overall low η of PZnSn ITPO SLP in comparison with that ITPO SA is attributed to the occurrence of a higher extent of intercalation reactions with low kinetics ITPO SLP. In the cases of both SA (Fig. 9c) and SLP (Fig. 10c), as the current density increases, η also increases and reaches the maximum of 100% at higher current densities during all points of cycling.

All the Nyquist plots of PZnSn obtained ITPO SA (Fig. 11a) contain a semicircle in a higher frequency region (HFR) and a linear Warburg portion in a lower frequency region (LFR), indicating the capacitive behavior of PZnSn ITPO SA. The resistance along the real axis of the Nyquist plots is associated with the series resistance of PZnSn. The series resistance is the sum of the solution resistance (R_s), charge-transfer resistance (R_{ct}),
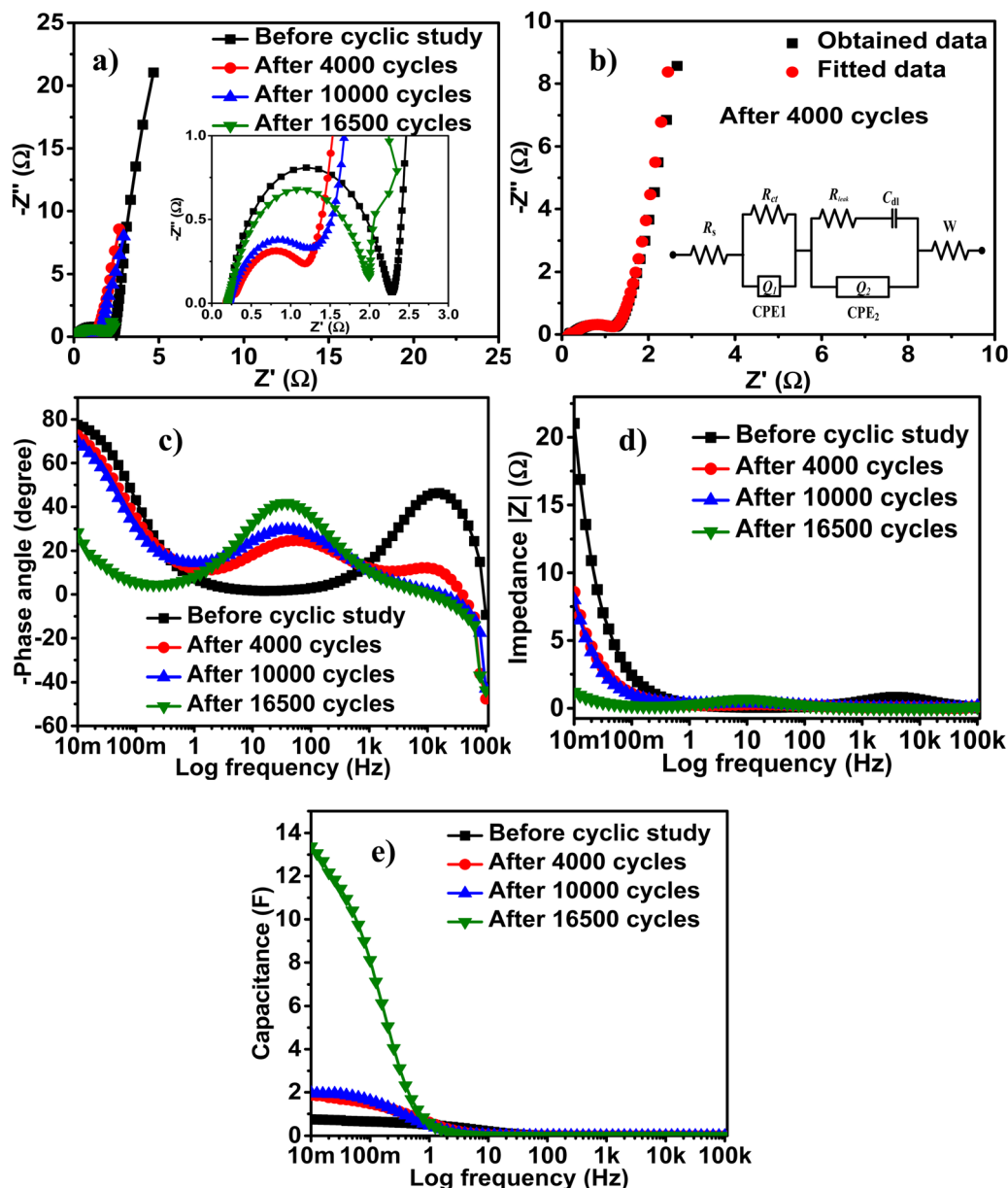
Fig. 11 (a) Nyquist plot, (b) EC fitted to Nyquist plot obtained after 4000 cycles, (c) Bode phase angle plots, (d) Bode impedance plots and (e) capacitance *vs.* log frequency plots of PZnSn obtained after DNC ITPO SA.

and Warburg diffusional resistance (W). This series resistance decreases with INC, indicating a reduction in overall resistance with INC ITPO SA.

The magnitudes of the electrical elements involved in the energy storage processes are obtained by fitting the equivalent circuit (EC) $R_s(R_{ct}Q_1)((R_{leak}C_{dl})(Q_2))W$ (Table 4 and Fig. 11b) to

the Nyquist plots obtained ITPO SA, and indicate that with INC R_s is decreasing, whereas R_{ct}, C_{dl} and W are increasing. Explanations of the electrical elements present in EC are provided in ESI.† The decrease in R_s and increase in C_{dl} are attributed to the enhancement in energy storage with INC. The increases in R_{ct} and W are accounted for by the increase in the drop of IR with

Table 4 The magnitudes of the electrical parameters of PZnSn composites obtained ITPO SA by equivalent circuit fitting of $R_s(R_{ct}Q_1)((R_{leak}C_{dl})(Q_2))W$

PZnSn	R_s (Ω)	R_{ct} (Ω)	Q_1 (F)	n_1	R_{leak} (Ω)	C_{dl} (F)	Q_2 (F)	n_2	W (Ω)
Before cyclic study	0.23	0.01	8.52×10^{-14}	0.80	2.10	0.79	1.18×10^{-4}	0.82	2.33
After 4000 cycles	0.19	0.3	2.10×10^{-3}	0.57	0.90	2.14	0.0358	0.71	2.35
After 10 000 cycles	0.21	1.13	0.0483	0.69	0.18	2.43	6.22×10^{-6}	0.99	2.53
After 16 500 cycles	0.20	1.77	0.0203	0.82	0.21	17.23	5.49×10^{-6}	0.99	11.38

INC and the reduction in η with INC ITPO SA. The lower drop in IR obtained before the cyclic stability study ITPO SA in relation to other points in the cyclic stability study is associated with its low R_{ct}. The increase in W with INC indicates an increase in resistance against the diffusion of electrolytic ions with INC, and this resistance is the reason behind the decrease in η with INC ITPO SA. The Bode phase angles (Fig. 11c) at LFR decrease with INC, indicating migration from the state of capacitor behavior to the state of supercapacitor behavior. The relaxation time (τ_o) (eqn (S10), ESI†) of PZnSn obtained before the cyclic study and after 4000 and 10 000 cycles are 0.81, 0.87 and 0.89 s, respectively. The phase angle plot obtained after 16 500 cycles did not reach the phase angle of $-45°$, and therefore, the τ_o after 16 500 cycles was left uncalculated. The increase in τ_o indicates the increase in energy storage with INC. The variation in Bode impedance plots obtained ITPO SA (Fig. 11d) with INC is in agreement with the variation in series resistance with INC. The decrease in overall resistance resulted in an overall increase in energy storage with INC (Fig. 9e). The impedance and capacitance (eqn (S11), ESI†) obtained ITPO SA at LFR of 0.01 Hz are 21.03, 8.57, 8.0, and 1.19 Ω, and 0.76, 1.86, 1.99, and 13.38 F, before the cyclic study and after 4000, 10 000 and 16 500 cycles, respectively.

Similarly, the EIS results of PZnSn ITPO SLP (Fig. 12) depict decreased resistance (Fig. 12a) with INC, indicating better diffusion of electrolytic ions and increased energy storage with

INC ITPO SLP. However, it is intriguing to note that the maximum performance was obtained after 10 000 cycles ITPO SLP, but the impedance (Fig. 12b) and the capacitance (Fig. 12c) corresponding to the EIS analysis after 5000 cycles are found to be the lowest and highest, respectively. This puzzle could be solved when the charge storage characters obtained after 5000 and 10 000 cycles ITPO SLP are compared. That is, the higher energy storage obtained after 10 000 cycles holds true only up to 3 A g^{-1}, after which all the Q that are obtained after 10 000 cycles are lower than those obtained after 5000 cycles. In addition, the rate capability and the tolerance to the higher current are found to be superior after 5000 cycles. Therefore, it is rational that PZnSn experiences lower impedance and stores higher energy after 5000 cycles ITPO SLP, which is seen in the EIS results of PZnSn obtained ITPO SLP. The magnitudes of the electrical elements that are obtained by fitting the same EC to the Nyquist plots of PZnSn that are obtained ITPO SLP after DNC (Table 5) evidently depict that with INC, the overall resistances are decreasing, the overall capacitances are increasing, and the least resistance and maximum capacitance are obtained after 5000 cycles. The rate capability and the coulombic efficiencies follow the same trend as that of W obtained after DNC. PZnSn exhibits maximum rate capability after 5000 cycles, as it possesses the lowest W at that point ITPO SLP.

To study the contributions and nature of the electrolytes used, their EIS studies were conducted by making devices that
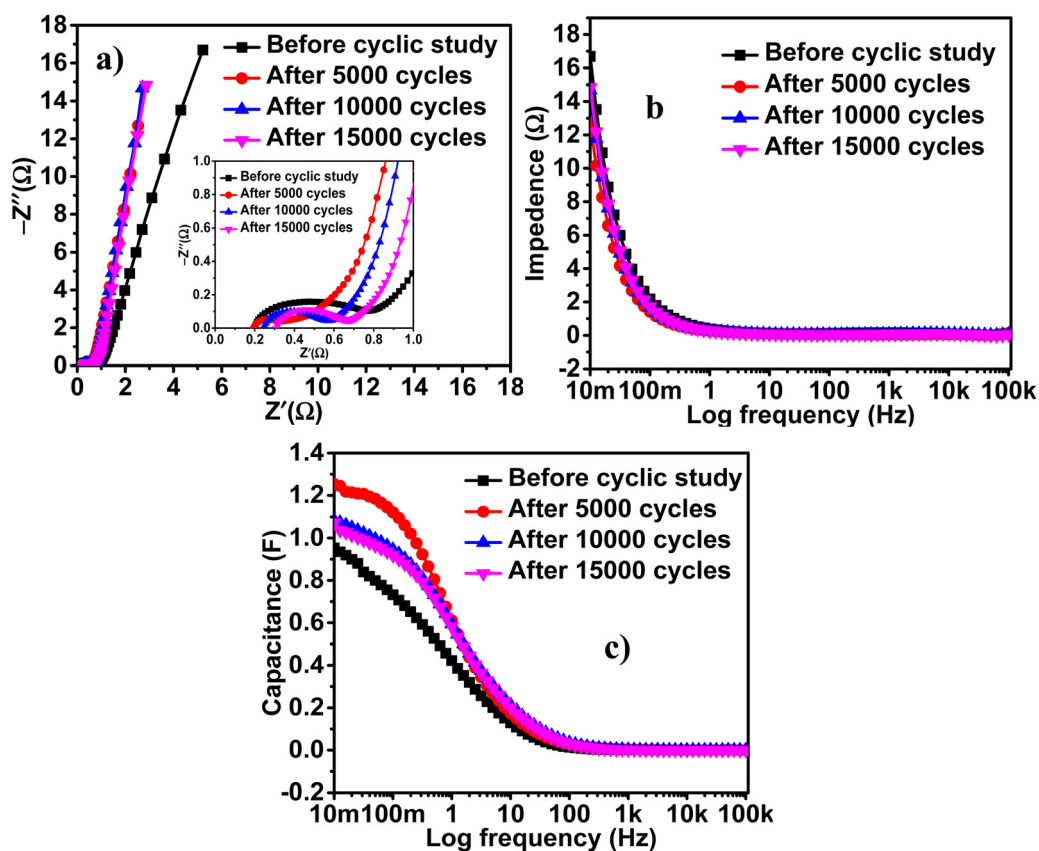

Fig. 12 (a) Nyquist plots, (b) Bode impedance plots and (d) capacitance vs. log frequency plots of PZnSn obtained after DNC ITPO SLP.

Table 5 The magnitudes of electrical parameters of PZnSn composites obtained ITPO SLP by equivalent circuit fitting of $R_s(R_{ct}Q_1)((R_{leak}C_{dl})(Q_2))W$

PZnSn	R_s (Ω)	R_{ct} (Ω)	Q_1 (F)	n_1	R_{leak} (Ω)	C_{dl} (F)	Q_2 (F)	n_2	W (Ω)
Before cyclic study	0.20	0.56	0.01	0.59	0.24	1.02	3.15×10^{-2}	0.35	4.45
After 5000 cycles	0.20	0.26	0.79	0.47	0.37	1.40	7.20×10^{-4}	0.47	2.19
After 10 000 cycles	0.25	0.08	1.25	0.64	0.37	1.20	3.35×10^{-3}	0.62	2.13
After 15 000 cycles	0.31	0.22	0.45	0.99	0.66	1.01	3.69×10^{-2}	0.35	2.19

Table 6 Comparison of energy storage performance of PZnSn with similar composites

Composite	Electrolyte	Potential window (V)	E (W h kg^{-1})	P (kW kg^{-1})	Cyclic stability	Ref.
2-EL systems						
PANI/ZnO/VO$_2$	1 M H$_2$SO$_4$	1.2	88.10 at 1 A g^{-1}	2.154	Good cyclic stability up to 16 812 cycles at 0.4 A g^{-1}	5
PANI/CuO/NiO	0.1 M Na$_2$SO$_4$	1.6	35.0 at 3.5 A g^{-1}	1.326	86% retention up to 10 000 cycles	59
PANI/CuO/SnO$_2$	1 M H$_2$SO$_4$	1.2	42.73 at 1 A g^{-1}	1.200	45.64% up retention to 5000 cycles at 0.4 V s^{-1}	44
PANI/CuO/SnO$_2$	1 M H$_2$SO$_4$ + 1 M CH$_3$SO$_3$H (1:1)	1.2	50.26 at 1 A g^{-1}	1.200	55.56% retention up to 12 500 cycles at 0.4 V s^{-1}	44
Present work PANI/ZnO/SnO$_2$	1 M H$_2$SO$_4$	1.2	52.00 at 1 A g^{-1}	1.200	No deterioration up to 16 500 cycles at 0.4 V s^{-1}	—
Present work PANI/ZnO/SnO$_2$	By-product of PANI	1.2	57.87 at 1 A g^{-1}	1.200	No deterioration up to 15 000 cycles at 0.4 V s^{-1}	—
3-EL systems						
PANI/Y$_2$O$_3$–ZnO	1 M KOH	1.0	73.08	9.135	94.9% retention up to 5000 cycles	60
PANI/Ag–ZnO	1 M H$_2$SO$_4$	0.8	88.00	0.4990	—	61

contain electrolytes (SA and SLP), separator and current collector without electrode material, and the findings are displayed in Fig. S10 (ESI†). As it can be seen, the Nyquist plots have a distorted semicircle and a Warburg portion (Fig. S10a, ESI†) showing the formation of a double layer at the solid (separator and current collector) and liquid (electrolyte) interface. The Bode impedance plots (Fig. S10b) and log frequency $vs.$ capacitance plots (Fig. S10c, ESI†) show that PZnSn exhibits lower impedance and higher capacitance ITPO of SLP, signifying its superiority to SA. The obtained impedance and capacitance ITPO SA and SLP are 4.862 and 4.127 kΩ, and 3.27 and 3.86 mF, respectively, at 0.01 Hz. The open circuit potential (OCP) obtained for these electrode-less devices are 167.4 mV and 206.7 mV ITPO SA and SLP, respectively. This high OCP obtained ITPO SLP indicates its lower internal resistance and higher ability to store energy in relation to that ITPO SA. Thus, the higher energy storage ITPO SLP is substantiated. A comparison of the performance of PZnSn with reported composites can be seen in Table 6, and the obtained results are comparable to or even better than those in some reports published elsewhere.

Conclusion

A composite, polyaniline/ZnO/SnO$_2$ of respective weight percentages of 58.34%:8.33%:33.33% (PZnSn), was synthesized in a facile $in~situ$ single-step method. The energy storage performance was evaluated with two aqueous electrolytes: 1 M H$_2$SO$_4$ (SA) and the liquid by-product that was obtained after the synthesis of PANI (SLP). SLP provided 57.25% higher energy storage performance than that provided by SA. PZnSn exhibited a durable and rate-capable energy storage property by exhibiting robustness up to 16 500 cycles at 0.4 V s^{-1} and 39 A g^{-1}, respectively, in the presence of (ITPO) SA and up to 15 000 cycles at 0.4 V s^{-1} and 42 A g^{-1} ITPO SLP, in a real-time symmetric two-electrode system. PZnSn displayed the remarkable trait of an enhancement in energy storage with an increase in charge and discharge cycles ITPO both electrolytes. However, the enhancement provided by SLP is higher than that provided by SA. The maximum performance achieved from PZnSn ITPO SLP is a Q of 347 C g^{-1}, an E of 57.87 W h kg^{-1} (comparable with Ni–Cd batteries) and a P of 1.2 kW kg^{-1} at 1 A g^{-1}. Therefore, PZnSn ITPO SLP would be suitable for fabricating hybrid supercapacitors providing high energy, high rate capability, and durability. The use of SLP in energy storage brings the entire work under the umbrella of "waste into wealth" and the concept of "green energy storage".

Data availability

The data generated during and/or analysed during the current study are available from the corresponding author on reasonable request.

Conflicts of interest

There are no conflicts to declare.

Acknowledgements

References

1 W. Chen, R. B. Rakhi and H. N. Alshareef, Facile Synthesis of Polyaniline Nanotubes Using Reactive Oxide Templates for High Energy Density Pseudocapacitors, *J. Mater. Chem. A*, 2013, **1**(10), 3315–3324, DOI: **10.1039/C3TA00499F**.

2 T. Liu, L. Finn, M. Yu, H. Wang, T. Zhai, X. Lu, Y. Tong and Y. Li, Polyaniline and Polypyrrole Pseudocapacitor Electrodes with Excellent Cycling Stability, *Nano Lett.*, 2014, **14**(5), 2522–2527, DOI: **10.1021/nl500255v**.

3 A. Viswanathan and A. N. Shetty, Influence of Different Dopants and Redox Forms of PANI in Its Crystal Structure, Morphology, Electrochemical Energy Storage to Variable Extent, Unique Properties and Kinetics, *Bull. Mater. Sci.*, 2022, **45**(2), 60, DOI: **10.1007/s12034-021-02626-9**.

4 Y. Chen and S. Manzhos, Voltage and Capacity Control of Polyaniline Based Organic Cathodes: An Ab Initio Study, *J. Power Sources*, 2016, **336**, 126–131, DOI: **10.1016/j.jpowsour.2016.10.066**.

5 A. Viswanathan and A. N. Shetty, Nanoporous PANI/ZnO/ VO_2 Ternary Nanocomposite and Its Electrolyte for Green Supercapacitance, *Mater. Sci. Eng. B*, 2024, **303**, 117322, DOI: **10.1016/j.mseb.2024.117322**.

6 B. Huang, X. Li, Y. Pei, S. Li, X. Cao, R. C. Massé and G. Cao, Novel Carbon-Encapsulated Porous SnO_2 Anode for Lithium-Ion Batteries with Much Improved Cyclic Stability, *Small*, 2016, **12**(14), 1945–1955, DOI: **10.1002/smll.201503419**.

7 S. M. Hwang, Y.-G. Lim, J.-G. Kim, Y.-U. Heo, J. H. Lim, Y. Yamauchi, M.-S. Park, Y.-J. Kim, S. X. Dou and J. H. Kim, A Case Study on Fibrous Porous SnO_2 Anode for Robust, High-Capacity Lithium-Ion Batteries, *Nano Energy*, 2014, **10**, 53–62, DOI: **10.1016/j.nanoen.2014.08.020**.

8 Y. Deng, C. Fang and G. Chen, The Developments of SnO_2/ Graphene Nanocomposites as Anode Materials for High Performance Lithium Ion Batteries: A Review, *J. Power Sources*, 2016, **304**, 81–101, DOI: **10.1016/j.jpowsour.2015.11.017**.

9 Z. Li and L. Gong, Research Progress on Applications of Polyaniline (PANI) for Electrochemical Energy Storage and Conversion, *Materials*, 2020, **13**(3), 548, DOI: **10.3390/ma13030548**.

10 C.-T. Hsieh, C.-Y. Lin, Y.-F. Chen and J.-S. Lin, Synthesis of ZnO@Graphene Composites as Anode Materials for Lithium Ion Batteries, *Electrochim. Acta*, 2013, **111**, 359–365, DOI: **10.1016/j.electacta.2013.07.197**.

11 C. Q. Zhang, J. P. Tu, Y. F. Yuan, X. H. Huang, X. T. Chen and F. Mao, Electrochemical Performances of Ni-Coated ZnO as an Anode Material for Lithium-Ion Batteries, *J. Electrochem. Soc.*, 2006, **154**(2), A65, DOI: **10.1149/1.2400609**.

12 X. H. Huang, X. H. Xia, Y. F. Yuan and F. Zhou, Porous ZnO Nanosheets Grown on Copper Substrates as Anodes for Lithium Ion Batteries, *Electrochim. Acta*, 2011, **56**(14), 4960–4965, DOI: **10.1016/j.electacta.2011.03.129**.

13 J. Zhang, P. Gu, J. Xu, H. Xue and H. Pang, High Performance of Electrochemical Lithium Storage Batteries: ZnO-Based Nanomaterials for Lithium-Ion and Lithium–Sulfur Batteries, *Nanoscale*, 2016, **8**(44), 18578–18595, DOI: **10.1039/C6NR07207K**.

14 K. K. Purushothaman, V. S. Priya, S. Nagamuthu, S. Vijayakumar and G. Muralidharan, Synthesising of ZnO Nanopetals for Supercapacitor Applications, *Micro Nano Lett.*, 2011, **6**(8), 668–670, DOI: **10.1049/mnl.2011.0260**.

15 M. Saranya, R. Ramachandran and F. Wang, Graphene-Zinc Oxide (G-ZnO) Nanocomposite for Electrochemical Supercapacitor Applications, *J. Sci.:Adv. Mater. Devices*, 2016, **1**(4), 454–460, DOI: **10.1016/j.jsamd.2016.10.001**.

16 D. Mohapatra, S. Parida, S. Badrayyana and B. K. Singh, High Performance Flexible Asymmetric CNO-ZnO//ZnO Supercapacitor with an Operating Voltage of 1.8 V in Aqueous Medium, *Appl. Mater. Today*, 2017, **7**, 212–221, DOI: **10.1016/j.apmt.2017.03.006**.

17 D. Kalpana, K. S. Omkumar, S. S. Kumar and N. G. Renganathan, A Novel High Power Symmetric ZnO/Carbon Aerogel Composite Electrode for Electrochemical Supercapacitor, *Electrochim. Acta*, 2006, **52**(3), 1309–1315, DOI: **10.1016/j.electacta.2006.07.032**.

18 A. U. Ammar, I. D. Yildirim, F. Bakan and E. Erdem, ZnO and MXenes as Electrode Materials for Supercapacitor Devices, *Beilstein J. Nanotechnol.*, 2021, **12**(1), 49–57, DOI: **10.3762/bjnano.12.4**.

19 C. Sasirekha, S. Arumugam and G. Muralidharan, Green Synthesis of ZnO/Carbon (ZnO/C) as an Electrode Material for Symmetric Supercapacitor Devices, *Appl. Surf. Sci.*, 2018, **449**, 521–527, DOI: **10.1016/j.apsusc.2018.01.172**.

20 A. Viswanathan and A. N. Shetty, High Energy and Rate Capable Supercapacitor of Polyaniline/Vanadium Pentoxide Nanocomposite and Its Green Electrolyte, *Next Sustainability*, 2025, **5**, 100088, DOI: **10.1016/j.nxsust.2024.100088**.

21 A. Viswanathan and A. N. Shetty, A Green Approach to Energy Storage Properties of Polyaniline, *Bull. Mater. Sci.*, 2024, **47**(4), 243, DOI: **10.1007/s12034-024-03329-7**.

22 A. Viswanathan and N. S. Adka, *Method and System for Synthesis of Electrode and Electrolyte Materials for High Energy Storage Devices. Indian Pat. Off.* 2023, *Application No. 201941044515* (Date of filing: 03/11/2019), Patent No. 450155.

23 H. R. Ghorbani, F. P. Mehr, H. Pazoki and B. M. Rahmani, Synthesis of ZnO Nanoparticles by Precipitation Method, *Orient. J. Chem.*, 2015, **31**(2), 1219–1221.

24 A. N. P. Madathil, K. A. Vanaja and M. K. Jayaraj, Synthesis of ZnO Nanoparticles by Hydrothermal Method, *Nanophotonic Materials IV*, SPIE, 2007, vol. 6639, pp. 47–55, DOI: **10.1117/12.730364**.

25 F. Wang, X. Qin, Z. Guo, Y. Meng, L. Yang and Y. Ming, Hydrothermal Synthesis of Dumbbell-Shaped ZnO Micro-structures, *Ceram. Int.*, 2013, **39**(8), 8969–8973, DOI: **10.1016/j.ceramint.2013.04.096**.

26 Y. Fang, Z. Li, S. Xu, D. Han and D. Lu, Optical Properties and Photocatalytic Activities of Spherical ZnO and Flower-like ZnO Structures Synthesized by Facile Hydrothermal Method, *J. Alloys Compd.*, 2013, **575**, 359–363, DOI: **10.1016/j.jallcom.2013.05.183**.

27 P. Chandrasekaran, G. Viruthagiri and N. Srinivasan, The Effect of Various Capping Agents on the Surface Modifications of Sol–Gel Synthesised ZnO Nanoparticles, *J. Alloys Compd.*, 2012, **540**, 89–93, DOI: **10.1016/j.jallcom.2012.06.032**.

28 S. K. Lim, S.-H. Hwang, S. Kim and H. Park, Preparation of ZnO Nanorods by Microemulsion Synthesis and Their Application as a CO Gas Sensor, *Sens. Actuators, B*, 2011, **160**(1), 94–98, DOI: **10.1016/j.snb.2011.07.018**.

29 L. Wan, S. Yan, J. Feng, Z. Yang, X. Fan, Z. Li and Z. Zou, Solvothermal Synthesis of Core–Shell ZnO Hollow Micro-hemispheres, *Colloids Surf., A*, 2012, **396**, 46–50, DOI: **10.1016/j.colsurfa.2011.12.039**.

30 S. Jiao, K. Zhang, S. Bai, H. Li, S. Gao, H. Li, J. Wang, Q. Yu, F. Guo and L. Zhao, Controlled Morphology Evolution of ZnO Nanostructures in the Electrochemical Deposition: From the Point of View of Chloride Ions, *Electrochim. Acta*, 2013, **111**, 64–70, DOI: **10.1016/j.electacta.2013.08.050**.

31 S. Yue, J. Lu and J. Zhang, Controlled Growth of Well-Aligned Hierarchical ZnO Arrays by a Wet Chemical Method, *Mater. Lett.*, 2009, **63**(24), 2149–2152, DOI: **10.1016/j.matlet.2009.06.055**.

32 M. Ushio and Y. Sumiyoshi, Synthesis of ZnO Single Crystals by the Flux Method, *J. Mater. Sci.*, 1993, **28**(1), 218–224, DOI: **10.1007/BF00349054**.

33 H. Wu and W. Pan, Preparation of Zinc Oxide Nanofibers by Electrospinning, *J. Am. Ceram. Soc.*, 2006, **89**(2), 699–701, DOI: **10.1111/j.1551-2916.2005.00735.x**.

34 M. Hasanpoor, M. Aliofkhazraei and H. Delavari, Microwave-Assisted Synthesis of Zinc Oxide Nanoparticles, *Procedia Mater. Sci.*, 2015, **11**, 320–325, DOI: **10.1016/j.mspro.2015.11.101**.

35 S. Lee, S. Jeong, D. Kim, S. Hwang, M. Jeon and J. Moon, ZnO Nanoparticles with Controlled Shapes and Sizes Prepared Using a Simple Polyol Synthesis, *Superlattices Microstruct.*, 2008, **43**(4), 330–339, DOI: **10.1016/j.spmi.2008.01.004**.

36 C. B. Ong, L. Y. Ng and A. W. Mohammad, A Review of ZnO Nanoparticles as Solar Photocatalysts: Synthesis, Mechanisms and Applications, *Renewable Sustainable Energy Rev.*, 2018, **81**, 536–551, DOI: **10.1016/j.rser.2017.08.020**.

37 S. Palsaniya, H. B. Nemade and A. K. Dasmahapatra, Hierarchical PANI-RGO-ZnO Ternary Nanocomposites for Symmetric Tandem Supercapacitor, *J. Phys. Chem. Solids*, 2021, **154**, 110081, DOI: **10.1016/j.jpcs.2021.110081**.

38 K. Pandiselvi and S. Thambidurai, Chitosan-ZnO/Polyaniline Ternary Nanocomposite for High-Performance Super-capacitor, *Ionics*, 2014, **20**(4), 551–561, DOI: **10.1007/s11581-013-1020-0**.

39 R. Karthik and S. Thambidurai, Synthesis of RGO–Co Doped ZnO/PANI Hybrid Composite for Supercapacitor Application, *J. Mater. Sci.:Mater. Electron.*, 2017, **28**(13), 9836–9851, DOI: **10.1007/s10854-017-6738-4**.

40 M. Naveed ur Rehman, T. Munawar, M. S. Nadeem, F. Mukhtar, U. A. Akbar, S. Manzoor, A. S. Hakeem, M. N. Ashiq and F. Iqbal, Facile Synthesis of Novel PANI Covered Y_2O_3–ZnO Nanocomposite: A Promising Electrode Material for Supercapacitor, *Solid State Sci.*, 2022, **128**, 106883, DOI: **10.1016/j.solidstatesciences.2022.106883**.

41 D. A. Tonpe, K. P. Gattu, V. V. Kutwade, S.-H. Han, B. R. Sathe and R. Sharma, ZnO-PANI Nanocomposite: Enhanced Electrochemical Performance towards Energy Storage, *J. Energy Storage*, 2024, **81**, 110434, DOI: **10.1016/j.est.2024.110434**.

42 D. Qin, B. Zhou, Z. Li and C. Yang, Construction of Controllable Multicomponent ZnO-ZnCo/MOF-PANI Composites for Supercapacitor Applications, *J. Mol. Struct.*, 2024, **1309**, 138140, DOI: **10.1016/j.molstruc.2024.138140**.

43 F. Decremps, J. Pellicer-Porres, A. M. Saitta, J.-C. Chervin and A. Polian, High-Pressure Raman Spectroscopy Study of Wurtzite ZnO, *Phys. Rev. B:Condens. Matter Mater. Phys.*, 2002, **65**(9), 092101, DOI: **10.1103/PhysRevB.65.092101**.

44 A. Viswanathan and A. N. Shetty, High Energy Supercapat-tery of Polyaniline/Cupric Oxide/Stannic Oxide Nanocomposite, *J. Phys. Chem. Solids*, 2024, **193**, 112141, DOI: **10.1016/j.jpcs.2024.112141**.

45 Y. Jin and M. Jia, Design and Synthesis of Nanostructured Graphene-SnO_2-Polyaniline Ternary Composite and Their Excellent Supercapacitor Performance, *Colloids Surf., A*, 2015, **464**, 17–25, DOI: **10.1016/j.colsurfa.2014.09.032**.

46 E. C. Onyiriuka, Zinc Phosphate Glass Surfaces Studied by XPS, *J. Non-Cryst. Solids*, 1993, **163**(3), 268–273, DOI: **10.1016/0022-3093(93)91304-L**.

47 J. Haber, J. Stoch and L. Ungier, X-Ray Photoelectron Spectra of Oxygen in Oxides of Co, Ni, Fe and Zn, *J. Electron Spectrosc. Relat. Phenom.*, 1976, **9**(5), 459–467, DOI: **10.1016/0368-2048(76)80064-3**.

48 S. W. Gaarenstroom and N. Winograd, Initial and Final State Effects in the ESCA Spectra of Cadmium and Silver Oxides, *J. Chem. Phys.*, 1977, **67**(8), 3500–3506, DOI: **10.1063/1.435347**.

49 J. Chastain and R. C. King Jr, Handbook of X-Ray Photoelectron Spectroscopy, *Perkin-Elmer Corp.*, 1992, **40**, 221.

50 M. Di Giulio, G. Micocci, A. Serra, A. Tepore, R. Rella and P. Siciliano, SnO_2 Thin Films for Gas Sensor Prepared by r.f. Reactive Sputtering, *Sens. Actuators, B*, 1995, **25**(1), 465–468, DOI: **10.1016/0925-4005(94)01397-7**.

51 W. Choi, H. Jung and S. Koh, Chemical Shifts and Optical Properties of Tin Oxide Films Grown by a Reactive Ion Assisted Deposition, *J. Vac. Sci. Technol., A*, 1996, **14**(2), 359–366, DOI: **10.1116/1.579901**.

52 J. C. C. Fan and J. B. Goodenough, X-ray Photoemission Spectroscopy Studies of Sn-doped Indium-oxide Films, *J. Appl. Phys.*, 1977, **48**(8), 3524–3531, DOI: **10.1063/1.324149**.

53 A. Viswanathan and A. N. Shetty, The High Energy Yielding Supercapattery of PANI/VO$_2$ Binary Nanocomposite, *Future Batteries*, 2024, **4**, 100009, DOI: **10.1016/j.fub.2024.100009**.

54 A. Viswanathan, M. G. Acharya, B. G. Prakashaiaha and A. N. Shetty, Superior Supercapacitance Exhibited by Acid Insoluble Ni(OH)$_2$ in the Form of Its Nanocomposite with rGO, *J. Energy Storage*, 2022, **55**, 105527, DOI: **10.1016/j.est.2022.105527**.

55 A. Viswanathan and A. N. Shetty, High Energy Supercapacitance of Magnetic PANI/Ni$_2$O$_3$ Nanocomposite and Its Magnetic Structural Repair, *J. Energy Storage*, 2024, **90**, 111759, DOI: **10.1016/j.est.2024.111759**.

56 A. Viswanathan and A. N. Shetty, Effect of Dopants on the Energy Storage Performance of Reduced Graphene Oxide/Polyaniline Nanocomposite, *Electrochim. Acta*, 2019, **327**, 135026, DOI: **10.1016/j.electacta.2019.135026**.

57 B. Dunn, B. Dunn, H. Kamath and J. Tarascon, Electrical Energy Storage for the Gridfor the Grid: A Battery of Choices, *Sci. Mag.*, 2011, **334**(6058), 928–936, DOI: **10.1126/science.1212741**.

58 T. Siva, K. Kamaraj and S. Sathiyanarayanan, Epoxy Curing by Polyaniline (PANI) – Characterization and Self-Healing Evaluation, *Prog. Org. Coat.*, 2014, **77**(6), 1095–1103, DOI: **10.1016/j.porgcoat.2014.03.019**.

59 S. M. Adnan, M. Shoeb, M. Z. Ansari, F. Mashkoor, M. Mobin, S. Zaidi and C. Jeong, Fabrication of NiO–CuO Decorated Polyaniline (PANI/NiO–CuO) Nanocomposite Based Symmetric Supercapacitor Device for High-Energy Density Performance with Wide Potential Window in Aqueous Electrolyte, *Inorg. Chem. Commun.*, 2023, **157**, 111265, DOI: **10.1016/j.inoche.2023.111265**.

60 M. Naveed ur Rehman, T. Munawar, M. S. Nadeem, F. Mukhtar, U. A. Akbar, S. Manzoor, A. S. Hakeem, M. N. Ashiq and F. Iqbal, Facile Synthesis of Novel PANI Covered Y$_2$O$_3$–ZnO Nanocomposite: A Promising Electrode Material for Supercapacitor, *Solid State Sci.*, 2022, **128**, 106883, DOI: **10.1016/j.solidstatesciences.2022.106883**.

61 B. Purty, R. B. Choudhary, R. Kandulna and R. Singh, Remarkable Enhancement in Electrochemical Capacitance Value of Ag-ZnO/PANI Composite for Supercapacitor Application, *AIP Conf. Proc.*, 2019, **2115**(1), 030588, DOI: **10.1063/1.5113427**.